JB
Journals.ASM.org

Biochemical Characterization of a Dihydroneopterin Aldolase Used for Methanopterin Biosynthesis in Methanogens

Yu Wang, Huimin Xu, Laura L. Grochowski, Robert H. White

Department of Biochemistry, Virginia Polytechnic Institute and State University, Blacksburg, Virginia, USA

The gene encoding 7,8-dihydroneopterin aldolase (DHNA) was recently identified in archaea through comparative genomics as being involved in methanopterin biosynthesis (V. Crécy-Lagard, G. Phillips, L. L. Grochowski, B. El Yacoubi, F. Jenney, M. W. Adams, A. G. Murzin, and R. H. White, ACS Chem. Biol. 7:1807–1816, 2012, doi:10.1021/cb300342u). Archaeal DHNA shows a unique secondary and quaternary structure compared with bacterial and plant DHNAs. Here, we report a detailed biochemical examination of DHNA from the methanogen *Methanocaldococcus jannaschii*. Kinetic studies show that *M. jannaschii* DHNA possesses a catalytic capability with a k_{cat}/K_m above 10^5 M^{-1} s^{-1} at 70°C, and at room temperature it exhibits a turnover number (0.07 s^{-1}) comparable to bacterial DHNAs. We also found that this enzyme follows an acid-base catalytic mechanism similar to the bacterial DHNAs, except when using alternative catalytic residues. We propose that in the absence of lysine, which is considered to be the general base in bacterial DHNAs, an invariant water molecule likely functions as the catalytic base, and the strictly conserved His35 and Gln61 residues serve as the hydrogen bond partners to adjust the basicity of the water molecule. Indeed, substitution of either His35 or Gln61 causes a 20-fold decrease in k_{cat}. An invariant Tyr78 is also shown to be important for catalysis, likely functioning as a general acid. Glu25 plays an important role in substrate binding, since replacing Glu25 by Gln caused a ≥25-fold increase in K_m. These results provide important insights into the catalytic mechanism of archaeal DHNAs.

Methanogenic archaea produce more than 350 million tons of methane each year, which is a substantial portion of the global carbon cycle (1). Tetrahydromethanopterin (H_4MPT; Fig. 1A) is the primary C_1 carrier coenzyme in the methanogenic pathway. Most methanogens do not have folate, the canonical C_1 carrier coenzyme, and instead use H_4MPT and its derivatives (2–4) for C_1 metabolism (5–7). Biosynthetic studies have revealed that methanopterin is distinct from folate on the basis of their different biosynthetic enzymes (8).

The biosynthetic pathway of methanopterin has been established, and many of the enzymes required for the biosynthesis of methanopterin in *Methanocaldococcus jannaschii* have been characterized (Fig. 1B) (9–13). Recently, a novel 7,8-dihydroneopterin aldolase (DHNA) belonging to the archaeal protein family COG2098 has been identified using a combination of comparative genomics analyses, heterologous complementation tests, and *in vitro* assays (14). The gene product of MJ0408, which is a member of the COG2098 protein family in *M. jannaschii*, has been cloned, heterologously expressed, and confirmed to be a DHNA (14). This enzyme is named MptD to indicate that it catalyzes the fourth step in methanopterin biosynthesis (Fig. 1B). The crystal structure of the MJ0408 gene product (Protein Data Bank [PDB] accession no. 2OGF), which was solved by Ramagopal et al. at the New York SGX Research Center for Structural Genomics, exhibits a distinctive secondary and quaternary structure compared to DHNAs from bacteria (15–17) and plants (18), indicating that it is apparently evolutionarily unrelated to other known aldolases.

Aldolases are generally divided into two classes based on their mechanism (19). Class I enzymes utilize the formation of a Schiff base between the ketogroup of the substrate and a conserved lysine residue in the active site to generate an iminium intermediate (20). The mechanism of class II enzymes utilizes Zn(II) as a Lewis acid and an active-site base for proton abstraction and formation of the enol intermediate (21) (Fig. 2). Bacterial DHNA is a unique class III aldolase since neither a Schiff base between the substrate and enzyme nor a metal ion is required for catalysis (22). Its proposed mechanism is similar to that seen in the class I enzymes, but the Schiff base is embedded in the substrate. The mechanism of bacterial DHNA has been studied (23, 24) and is expected to involve the formation of the enamine intermediate from the imine in the D-7,8-dihydroneopterin (DHNP) substrate. Mutagenesis studies with enzymes from *Escherichia coli* and *Staphylococcus aureus* implicated a conserved lysine and glutamate residue as being involved in the catalytic mechanism, with the lysine acting as the catalytic base, which is required to deprotonate the 2′-hydroxyl of DHNP (15, 23, 24).

It has been proposed that archaeal DHNA may have a similar enzymatic mechanism (14). However, the available crystal structures of the COG2098 protein family (PDB accession no. 2IEC, 2I52, and 2OGF) show no conserved lysine residue in the active site to serve as a catalytic base. Instead, two tyrosines, one glutamine, and one histidine at the active-site pocket are possibly involved in catalysis. In addition, an invariant glutamic acid may serve as an anchor for the bound substrate as revealed by the crystal structure (PDB accession no. 2OGF). In this report, we characterize DHNA from *M. jannaschii* by steady-state and pH-dependent kinetic studies. Then, we describe a site-directed mutagenesis study of five conserved amino acid residues to determine their functional roles. These results provide important insight into

Received 2 May 2014 Accepted 20 June 2014
Published ahead of print 30 June 2014
Address correspondence to Robert H. White, rhwhite@vt.edu.
Supplemental material for this article may be found at http://dx.doi.org/10.1128/JB.01812-14.

doi:10.1128/JB.01812-14

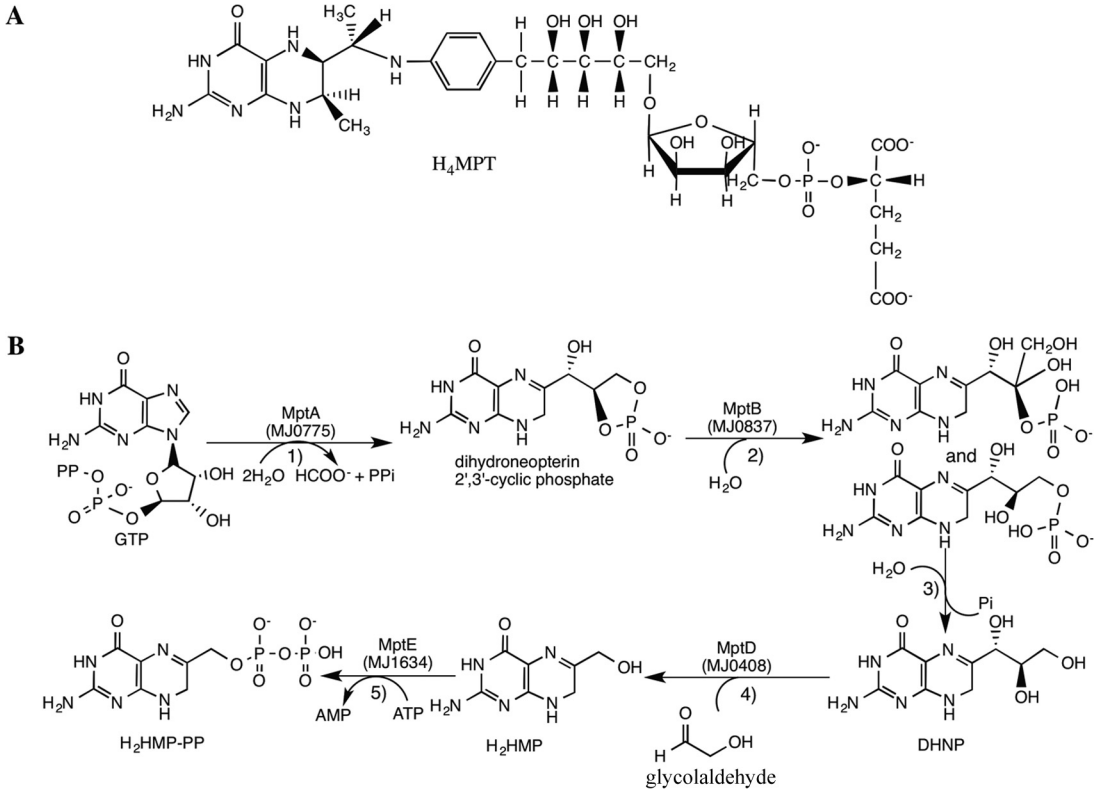

FIG 1 (A) The structure of tetrahydromethanopterin (H_4MPT); (B) biosynthesis of the pterin portion of methanopterin. DHNP, 7,8-dihydroneopterin; H_2HMP, 7,8-dihydro-6-hydroxymethylpterin; H_2HMP-PP, 7,8-dihydro-6-hydroxymethylpterin pyrophosphate.

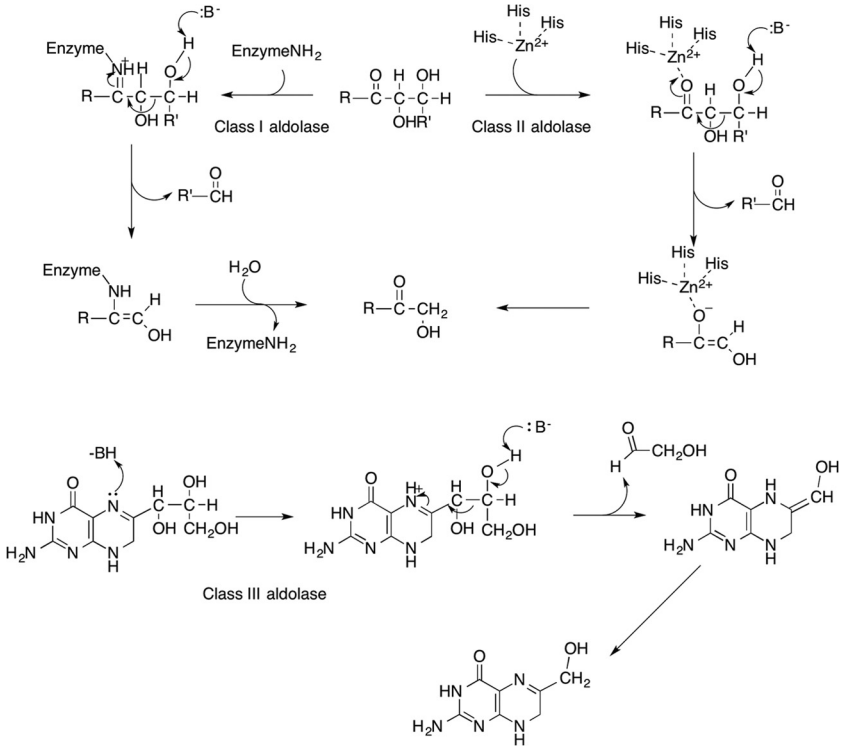

FIG 2 Reaction mechanisms for class I, II, and III aldolases.

the catalytic mechanism of the archaeal DHNA and also offer an excellent example of enzyme convergent/parallel evolution.

MATERIALS AND METHODS

Chemicals. 7,8-Dihydro-6-hydroxymethylpterin, 6-hydroxymethylpterin, D-neopterin, and L-monapterin were purchased from Schircks Laboratories (Jona, Switzerland). D-7,8-Dihydroneopterin and other chemicals were obtained from Sigma-Aldrich.

Preparation of *M. jannaschii* cell extracts. Cell extracts of *M. jannaschii* were prepared by sonication under argon and stored as previously described under anaerobic conditions at −20°C (25). The buffer used in the extraction was 50 mM *N*-tris(hydroxymethyl)methyl-2-aminoethanesulfonic acid (TES)-K^+ (pH 7.5), 10 mM $MgCl_2$, and 20 mM dithiothreitol (DTT), kept under argon.

Partial purification of DHNA activity from *M. jannaschii*. Partial purification of the DHNA activity from *M. jannaschii* was performed by sequential anion exchange and size exclusion chromatography using the assay described below. The soluble fraction of *M. jannaschii* cell extract was applied to a MonoQ anion exchange column (1 by 8 cm) equilibrated with 25 mM Tris-HCl (pH 7.5) and eluted with a linear gradient from 0 to 1 M NaCl in 25 mM Tris-HCl (pH 7.5) over 55 ml at 1 ml/min.

Cloning and expression of *M. jannaschii* MJ0408 and generation of *M. jannaschii* MJ0408 mutants. The *M. jannaschii* gene at locus MJ0408 (Swiss-Prot accession no. Q57851) was recombinantly produced and expressed as previously described (14). The Quick-Change TM site-directed mutagenesis kit (Stratagene) was used to construct MJ0408 mutants according to the manufacturer's instructions using template pMJ0408. Primers used for the mutants are listed in Table S1 in the supplemental material. The sequences of plasmids carrying the MJ0408 gene and its mutations were confirmed by sequencing (DNA Facility of Iowa University).

Purification and identification of recombinant *M. jannaschii* DHNA. The gene products of MJ0408 and its variants were purified as previously described (14). Protein concentration was determined by Bradford analysis (26). The identity of the purified enzyme was verified by matrix-assisted laser desorption ionization mass spectral analysis (MALDI-MS) of the excised protein band from the polyacrylamide gel, following in-gel trypsin digestion, using a 4800 time of flight (TOF/TOF) mass spectrometer (Applied Biosystems).

Steady-state kinetic study of *M. jannaschii* DHNA. Determination of kinetic parameters was conducted by measuring DHNA specific activity in a 100-μl reaction volume, where one of the enzymes (15 ng wild type, 40 ng Y111F variant, 500 ng H35N, Y78F, Q61A, and E25Q variants) was incubated with various DHNP concentrations (1 to 200 μM) in 100 mM TES, pH 7.6 (pH measured at 70°C), for 10 min at 70°C. To measure the reverse reaction, the DHNP and/or 7,8-dihydromonapterin (DHMP) formation was measured in a 100-μl reaction volume, including 700 ng wild-type *M. jannaschii* DHNA, 100 μM 7,8-dihydro-6-hydroxymethylpterin (H_2HMP), and 1 to 50 mM glycolaldehyde under the same conditions as those described above. The oxygenase activity was monitored by the formation of 7,8-dihydroxanthopterin (DHXP) under the same reaction conditions. For the activity obtained at 25°C, 500 ng of wild-type enzyme was incubated with various DHNP concentrations (1 to 200 μM) for 30 min in 100 mM TES, pH 7.6 (pH measured at 25°C).

Following incubation, the reactions were quenched by the addition of 10 μl 1 M trichloroacetic acid (TCA), and the precipitant was removed by centrifugation and then neutralized by adding 8.3 μl 1.5 M (pH 8.8) Tris buffer. DHNP, H_2HMP, DHMP, and DHXP in the incubation mixture were oxidized to fluorescent neopterin, 6-hydroxymethylpterin, monapterin, and xanthopterin, respectively, by the addition of 5 to 10 μl of a saturated solution of iodine in methanol and incubated at room temperature for 10 min. Following oxidation, the excess iodine was removed by reduction with 5 to 8 μl 1 M $NaHSO_3$. The resulting samples were analyzed by high-performance liquid chromatography (HPLC). Measurement of the extent of the reaction at each time point was based on the ratios of the measured areas of the fluorescence intensity of the neopterin and 6-hydroxymethylpterin peaks. From these ratios and from the known concentration of neopterin, the concentration of the product was calculated. This procedure was shown to be valid since the quantum yields for both compounds were found to be identical.

HPLC analysis of pterins. Chromatographic separation of pterins was performed on a Shimadzu UFLC system equipped with a C_{18} reverse phase column (Varian Pursuit XRs; 250 by 4.6 mm, 5-μm particle size). The elution profile consisted of 5 min at 95% sodium acetate buffer (25 mM, pH 6.0, in the presence of 0.02% NaN_3) and 5% methanol followed by a linear gradient to 45% sodium acetate buffer-55% methanol over 20 min at 1.0 ml/min. Pterins were detected by fluorescence using an excitation wavelength of 356 nm and an emission wavelength of 450 nm.

pH-dependent kinetic study. To investigate the role of acid-base catalysis in the *M. jannaschii* DHNA-catalyzed aldolase reaction, the pH-dependent kinetic parameters were obtained by measuring the rate of H_2HMP formation at various pHs. In a 100-μl volume, 15 ng wild-type enzyme (500 ng H35N or Y78F variant) was incubated in 25 mM tricine-CAPS-TES buffer from pH 5.9 to 10.5 (pH values measured at 70°C). At each pH, the enzyme was reacted with various DHNP concentrations (1 to 200 μM) at 70°C for 10 min. The k_{cat}/K_m was calculated by fitting the data to the Michaelis-Menten equation. The pH profiles of the wild-type and H35N enzymes were fitted to equation 1, and the pH profile of the Y78F enzyme was fitted to equation 2, using Prism 5.0c, where Y is the kinetic parameter (here Y is equal to k_{cat}/K_m), x is the pH, C is the pH-independent value of Y, and K_{a1} and K_{a2} are the apparent basic and acidic dissociation constants, respectively.

$$Y = \frac{C}{1 + \frac{10^{-x}}{10^{-K_{a1}}} + \frac{10^{-K_{a2}}}{10^{-x}}} \quad (1)$$

$$Y = \frac{C}{1 + \frac{10^{-x}}{10^{-K_{a1}}}} \quad (2)$$

RESULTS

Recombinant expression and purification of *M. jannaschii* DHNA. DHNA was partially purified from *M. jannaschii* cell extracts by anion exchange chromatography, and enzymatic activity was detected in the fractions eluting at 150 mM NaCl. This elution position was the same as that observed with the recombinant protein. Native DHNA from *M. jannaschii* was purified only partially due to the relatively low abundance of enzyme in the cells.

The MJ0408 gene product encoding DHNA was overexpressed in *E. coli* and purified by heating the cell extract to 80°C followed by anion exchange chromatography. The resulting protein (approximately 14 kDa) was greater than 95% pure as evaluated by SDS-PAGE (see Fig. S1 in the supplemental material). The identity of the purified protein was confirmed by MALDI-MS of the tryptic-digested protein band. The purified recombinant protein was confirmed to be a DHNA, as it was found to catalyze the formation of H_2HMP from DHNP (Fig. 1B, reaction 4) (14). The wild-type DHNA and its five variants were all found to possess high thermal stability and retained their activities following heating at 80°C for 20 min. Moreover, they all exhibited good stability at high pH, since no protein aggregation or precipitation was observed when proteins were incubated for 10 min at 70°C in 25 mM tricine-CAPS-TES buffer at pH 10.5.

Detection of other enzymatic activities of the *M. jannaschii* DHNA. Bacterial DHNAs are capable of catalyzing the epimerization of DHNP to DHMP (27–29). This epimerization activity was also observed with archaeal DHNA, as evidenced by the appearance of a small new peak upon HPLC analysis, which corre-

TABLE 1 Steady-state kinetic parameters of *M. jannaschii* DHNA and its variants

DHNA enzyme	Value at pH 7.6		
	k_{cat} (s^{-1})	K_m (μM)	k_{cat}/K_m (M^{-1} s^{-1})
Wild type (25°C)[a]	0.07 ± 0.01	64.5 ± 10	1.1×10^3
Wild type[b]	1.0 ± 0.1	9.9 ± 2	1.0×10^5
E25Q variant[b]	0.68 ± 0.05	≥250	≤2.7×10^3
H35N variant[b]	0.055 ± 0.005	21 ± 5	2.6×10^3
Q61A variant[b]	0.048 ± 0.004	8.4 ± 2	5.7×10^3
Y78F variant[b]	0.054 ± 0.006	30 ± 10	1.8×10^3
Y111F variant[b]	0.64 ± 0.02	11 ± 1	5.8×10^4

[a] Kinetic parameters were conducted by measuring DHNA-specific activity in a 100-μl reaction volume including 500 ng wild-type DHNA in 100 mM TES buffer at pH 7.6 (25°C), with varying DHNP concentrations (1 to 200 μM) for 30 min at 25°C.
[b] Kinetic parameters were conducted by measuring DHNA specific activity in a 100-μl reaction volume, including 15 ng wild type, 40 ng Y111F variant, or 500 ng H35N variant, Y78F variant, Q61A variant, or E25Q variant in 100 mM TES buffer at pH 7.6 (70°C), with varying DHNP concentrations (1 to 200 μM) for 10 min at 70°C.

sponded to monapterin. However, the amount of monapterin was less than 1% compared to the major product 6-hydroxymethylpterin. Recently, it has been shown that wild-type DHNA from *Mycobacterium tuberculosis* (27), the Y54F variant from *S. aureus*, and the Y53F variant from *E. coli* (30) possess oxygenase activity, where DHNP is converted to DHXP. However, for *M. jannaschii* DHNA, oxygenase activity was not detected with the wild-type enzyme or with the tested variants.

Reversibility of *M. jannaschii* DHNA. Aldolase-catalyzed reactions are generally reversible. Bacterial DHNAs have been shown to be reversible using millimolar glycolaldehyde (24, 27), with an apparent K_m for glycolaldehyde of ~10 mM. Similarly, the reverse reaction was observed here with *M. jannaschii* DHNA when using glycolaldehyde of ≥50 mM. Following oxidation, two peaks representing neopterin (4.8 min) and monapterin (5.8 min) were generated by the reverse reaction, as observed by HPLC (see Fig. S2 in the supplemental material).

Steady-state kinetic study. The catalytic properties of wild-type DHNA and five variants were determined from the steady-state kinetic measurements, and kinetic parameters are listed in Table 1. The DHNA from *M. jannaschii* exhibited a turnover number (0.07 s^{-1} at 25°C) comparable to that of bacterial DHNAs, which have reported turnover numbers ranging from 0.005 to 0.08 s^{-1}. However, its K_m is 10- to 500-fold higher than those of bacterial DHNAs (23, 27).

M. jannaschii cells grow in an environment where the temperature ranges from 48°C to 94°C (31). Consistent with this, wild-type DHNA and its five variants were all found to possess high thermal stability. To evaluate the catalytic abilities of *M. jannaschii* DHNA at temperatures similar to its physiological growth temperature, the steady-state kinetic studies were performed at 70°C. At this temperature, *M. jannaschii* DHNA exhibited higher catalytic abilities than those measured at 25°C, with a turnover number of 1.0 s^{-1} and a k_{cat}/K_m above 10^5 M^{-1} s^{-1} (Table 1). Notably, the K_m value was 6-fold smaller at 70°C than that at 25°C, which has been observed for other archaeal thermophilic enzymes, possibly due to a temperature-dependent conformational change (32).

In addition, enzyme assays conducted in the presence of 200 μM divalent metals (Fe, Mn, Cu, Co, Ni, Mg, or Zn) or 5 mM EDTA did not alter either k_{cat} or K_m (results not shown here), indicating that *M. jannaschii* DHNA is a metal-independent enzyme.

Single substitution of Tyr111 with phenylalanine caused a 40% decrease in k_{cat}. In contrast, H35N, Q61A, and Y78F variants all showed about 20-fold decreases in k_{cat}, indicating that these residues are important for catalysis (Table 1). Notably, replacing His35 or Tyr78 caused slight increases in K_m. In contrast, substitution of Glu25 with Gln caused a 25-fold increase in K_m, indicating that Glu25 is important for substrate binding.

pH-dependent kinetic study. DHNAs from bacteria are cofactor and metal independent. As a result, the mechanism for catalyzing the cleavage of a carbon-carbon bond was proposed based on general acid-base catalysis (23, 24). DHNA from *M. jannaschii* is also cofactor and metal independent. Therefore, it is reasonable to propose that the DHNA from *M. jannaschii* follows a similar general acid-base catalysis mechanism. In this study, pH profiles of k_{cat}/K_m were evaluated. The k_{cat}/K_m of the wild-type *M. jannaschii* DHNA exhibited a bell-shaped dependence on pH with the

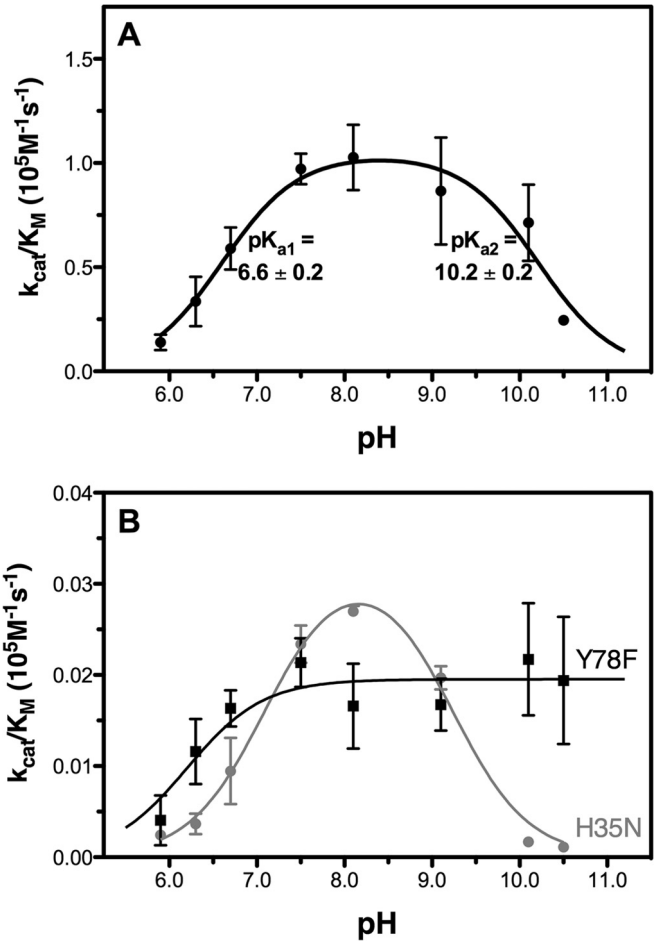

FIG 3 (A) pH dependence of k_{cat}/K_m for wild-type DHNA from *M. jannaschii*; (B) pH dependence of k_{cat}/K_m for the H35N and Y78F variants. Data were obtained by measuring the rate of product formation at various pHs by incubating 15 ng of wild-type DHNA (500 ng H35N or Y78F variant) in 25 mM TES-tricine-CAPS buffer from pH 5.9 to 10.5; at each pH, the enzyme reacted with various DHNP concentrations (1 to 200 μM) for 10 min at 70°C. The k_{cat}/K_m was calculated by fitting the data to the Michaelis-Menten equation, and the pH profiles of wild-type and H35N enzymes were fitted to equation 1, and the pH profile of the Y78F enzyme was fitted to equation 2.

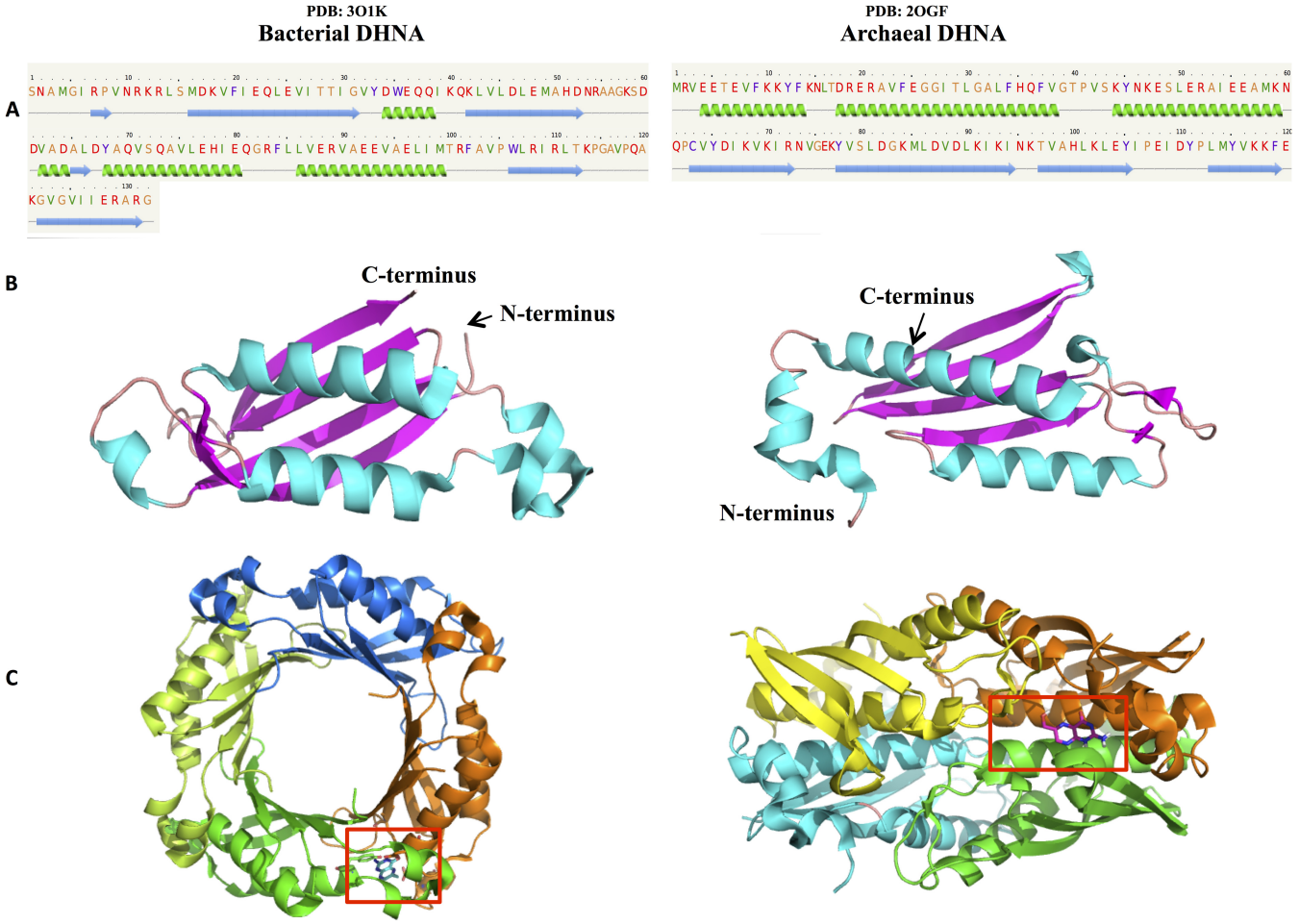

FIG 4 (A) Comparison of bacterial (left) and archaeal (right) DHNAs at the levels of protein sequence and secondary structure assignment (blue arrows represent β-sheet structure, green helices represent α-helices; the secondary structure assignment was performed by Phyre2 [38]); (B) secondary structure (cyan highlights α-helices while hot pink represents β-sheet); (C) quaternary structure (the four different colors highlight four identical subunits). Two bacterial DHNA tetrameric rings "head to head" stack together and assemble into a hollow cylinder octamer. Only one tetrameric ring is shown here. For archaeal DHNA, four subunits assemble into a compact homotetramer instead. Red boxes indicate the locations of the active sites.

optimum around pH 7.5 to 8.5 (Fig. 3A), having an apparent pK_{a1} of ~6.6 and an apparent pK_{a2} of ~10.2 by fitting equation 1. The pH dependency of k_{cat}/K_m reflects the ionization of free enzyme or free substrate (27–29). Thus, the two apparent pK_as might reflect the ionization of His35 and Tyr78, respectively. To test this hypothesis, the pH profiles of k_{cat}/K_m were also evaluated for the H35N and Y78F variants. For the H35N variant, a bell-shaped pH dependence was observed, with an apparent pK_{a1} of ~7.1 and an apparent pK_{a2} of ~9.2 (Fig. 3B). This indicates that the pK_{a1} of the wild-type DHNA is unlikely to reflect the ionization of His35. Notably, substitution of Tyr78 caused a significant change in the pH profile, in which only one pK_a (~6.4) was observed. Therefore, the pK_{a2} observed in the wild-type DHNA reflects the ionization of Tyr78, indicating that it serves as a general acid during catalysis.

DISCUSSION

Archaeal DHNAs (COG2098 protein family) share no sequence resemblance with bacterial and plant DHNAs. At first glance, the folding of archaeal DHNAs has similar features to bacterial DHNAs, in that each subunit comprises two main α-helices and a four-stranded β-sheet. However, the topological arrangement of these secondary structures is in a quite different order (14) (Fig. 4A and B). For bacterial DHNA, each subunit starts and ends with two β-sheets, with the two main α-helices located in between those β-sheets. In contrast, for archaeal DHNA, the two main α-helices are located at the N terminus and a four-stranded β-sheet is at the C terminus. At the quaternary structure level, four archaeal DHNA subunits assemble into a compact homotetramer, unlike the ring-shaped octamer architecture found in bacterial DHNAs (15–17) (Fig. 4C).

Sequence alignment shows that there are several strictly conserved residues among archaeal DHNAs (see Fig. S3 in the supplemental material). Of these, Glu25, His35, Gln61, and Tyr78 are located around the putative active sites, where a ligand tentatively identified as 8-oxoguanine has been found in *M. jannaschii* DHNA (PDB accession no. 2OGF). By docking the product H_2HMP in this active site, we observed that the H_2HMP molecule fits perfectly into the active-site pocket (Fig. 5). Glu25 is in a similar orientation as the Glu74 from *S. aureus* DHNA, which is believed to be responsible for substrate binding and stabilizing the

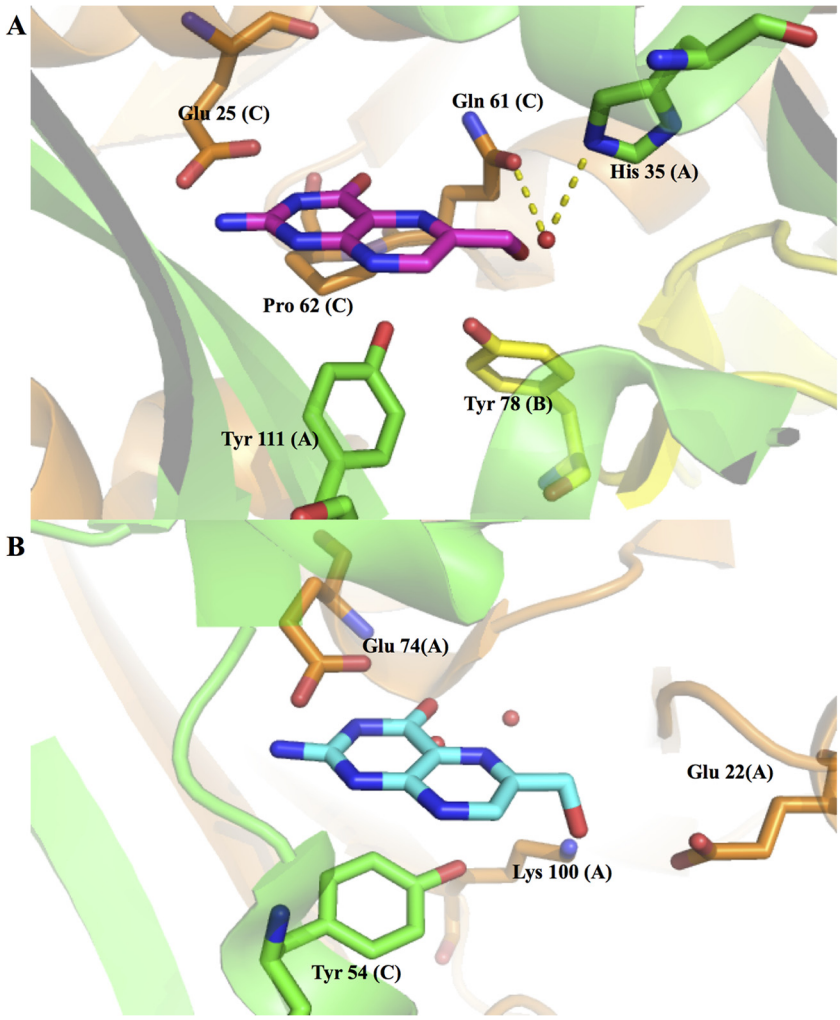

FIG 5 Comparison of the active sites of archaeal (A) and bacterial (B) DHNAs. In panel A, the protein coordinates are from the structure of *M. jannaschii* DHNA (PDB accession no. 2OGF). The product molecule H_2HMP (from PDB accession no. 1HQ2) was docked to the DHNA putative active site by Autodock Vina built-in Chimera (39, 40). Secondary structures and residues in green are from subunit A; those in orange are from subunit C; and Tyr 78, highlighted in yellow, is from subunit B. In panel B, coordinates are for the structure of bacterial DHNA from *Vibrio cholerae* O1 biovar El Tor strain N16961 (PDB accession no. 3O1K with aligned H_2HMP [PDB accession no. 2DHN] in the active site). Numbering reflects the DHNA from *S. aureus*. Secondary structures in green are from subunit C, and those in orange are from subunit A. Red spheres represent water molecules. Dotted lines indicate inferred polar contacts.

N5-protonated substrate in the binary complex (15, 23). It is reasonable to assume that Glu25 from *M. jannaschii* DHNA plays a similar role. Replacement of this corresponding glutamic acid in bacterial DHNA causes a significant increase in K_m (23). Similarly, the E25Q variant exhibited a K_m of ~250 μM, which is 25-fold higher than that of the wild-type enzyme, further indicating that Glu25 is an anchor for substrate binding.

The available crystal structures of archaeal DHNAs reveal that other residues that are possibly responsible for substrate binding or catalysis are Gln61, Pro62, Tyr78, and Tyr111 (Fig. 5). In the structure of bacterial DHNAs, a conserved tyrosine residue (Y54 in *S. aureus* DHNA) appears at almost the same position as Y111 in *M. jannaschii* DHNA (Fig. 5), and it has been proposed to act as a catalytic acid in the protonation of the enol intermediate (30). A point mutation of this tyrosine converts DHNA into an oxygenase (30). This tyrosine could also be modulating water accessibility to the active site, which is required to protonate the N5 of DHNP (27). However, this tyrosine's roles in *M. jannaschii* DHNA catalysis and substrate binding are not immediately obvious, and its precise role needs further investigation. Replacement of Tyr111 by Phe retained at least half of the activity, indicating that its role in catalysis is minor and that it is unlikely that it functions as an acid catalyst. Importantly, no oxygenase activity is observed in Y111F in *M. jannaschii* DHNA. This tyrosine is naturally replaced by phenylalanine in a few of the COG2098 family members (see Fig. S3 in the supplemental material).

It has been proposed that the bacterial and plant DHNAs follow a general acid and base catalytic mechanism (15, 23, 24, 27, 28). An invariant lysine acts as a general base, which abstracts the proton of the 2′-OH group, initiating cleavage of the C1′-C2′ carbon bond. Archaeal DHNA lacks such a lysine residue in the active site. At first glance, a strictly conserved histidine is the best candidate for acting as a general base. However, the pH profile of H35N showed a bell shape similar to that of the wild type, indicating that other residues or water molecules might serve as the catalytic base. By examining the available crystal structures,

an invariant water molecule was found to appear at the edge of the 2′-OH group of DHNP (around 1 Å away) and likely plays such a role. The strictly conserved His35 and Gln61 form a hydrogen-bonded network with this water molecule, assisting its ability to abstract a proton from the 2′-OH group of DHNP. Indeed, substitution of either His35 or Gln61 caused a similar influence on k_{cat}.

Another difference at the active site between archaeal and bacterial DHNA is that the archaeal DHNA possesses an invariant tyrosine (Tyr78) in subunit B (Fig. 5). Bacterial DHNA's active site is located at the interface of two adjacent subunits (Fig. 4C). Residues from both subunits contribute to substrate binding and catalysis. In contrast, the quaternary structure of archaeal DHNA is more compact, allowing residues from three subunits to contribute to the active site. Although Tyr78 is 3.9 Å away from the N5 of DHNP, the temperature-induced or substrate-induced conformational change might allow Tyr78 to donate a proton for the formation of an enol intermediate. Indeed, substitution of Tyr78 with Phe caused the k_{cat}/K_m to decrease by 2 orders of magnitude, and the Y78F variant exhibited a pH profile, which lacked a pKa_2, further suggesting that Tyr78 serves as a catalytic acid during catalysis. Interestingly, this tyrosine is missing in bacterial DHNAs; instead, a water molecule is believed to serve as the proton donor. Although tyrosine is not a common general acid, it has been shown to function as a general acid catalyst in the mechanism of ketosteroid isomerase (33, 34) and aldose reductase (35). Moreover, it has been reported that Tyr/Glu/His usually function as general acid/base residues involved in Schiff base chemistry (36).

In summary, although the catalytic chemistries of archaeal and bacterial DHNAs are essentially equivalent, archaeal DHNAs employ distinctive catalytic residues and exhibit unique structural folding. Comparison of their active-site architecture, protein folding, and catalytic abilities provides a perspective of DHNA evolution. In particular, archaeal and bacterial DHNAs represent a remarkable example of enzyme convergent/parallel evolution (37).

ACKNOWLEDGMENTS

This work was supported by funds from the National Science Foundation MCB 0722787 and 1120346 grants to R.H.W.

We thank Walter Niehaus, Janet Webster, and Kylie Allen for invaluable discussions. We also thank Keith Ray for obtaining the MALDI mass spectral data. The mass spectrometry resources are maintained by the Virginia Tech Mass Spectrometry Incubator, a facility operated in part through funding by the Fralin Life Science Institute at Virginia Tech and by the Agricultural Experiment Station Hatch Program (CRIS project number VA-135981).

REFERENCES

1. **Neue H.** 1993. Methane emissions from rice fields. Bioscience **43:**466–476. http://dx.doi.org/10.2307/1311906.
2. **Ferry JG.** 1999. Enzymology of one-carbon metabolism in methanogenic pathways. FEMS Microbiol. Rev. **23:**13–38. http://dx.doi.org/10.1111/j.1574-6976.1999.tb00390.x.
3. **Deppenmeier U.** 2002. The unique biochemistry of methanogenesis. Prog. Nucleic Acid Res. Mol. Biol. **71:**223–283. http://dx.doi.org/10.1016/S0079-6603(02)71045-3.
4. **White RH.** 1997. Structural characterization of modified folates in *Archaea*. Methods Enzymol. **281:**391–401. http://dx.doi.org/10.1016/S0076-6879(97)81046-4.
5. **Delle Fratte S, White RH, Maras B, Bossa F, Schirch V.** 1997. Purification and properties of serine hydroxymethyltransferase from *Sulfolobus solfataricus*. J. Bacteriol. **179:**7456–7461.
6. **Nyce GW, White RH.** 1996. dTMP biosynthesis in archaea. J. Bacteriol. **178:**914–916.
7. **Krone UE, McFarlan SC, Hogenkamp HP.** 1994. Purification and partial characterization of a putative thymidylate synthase from *Methanobacterium thermoautotrophicum*. Eur. J. Biochem. **220:**789–794. http://dx.doi.org/10.1111/j.1432-1033.1994.tb18680.x.
8. **Grochowski LL, White RH.** 2010. Biosynthesis of the methanogenic coenzymes, p 711–748. *In* Begley T (ed), Comprehensive natural products chemistry II: cofactor biosynthesis and enzymology. Elsevier, New York, NY.
9. **Grochowski LL, White RH.** 2010. Biosynthesis of the methanogenic coenzymes, p 711–748. *In* Begley TP (ed), Comprehensive natural products II: chemistry and biology, vol 7. Elsevier, New York, NY.
10. **Grochowski LL, Xu H, Leung K, White RH.** 2007. Characterization of an Fe^{2+}-dependent archaeal specific GTP cyclohydrolase, MptA, from *Methanocaldococcus jannaschii*. Biochemistry **46:**6658–6667. http://dx.doi.org/10.1021/bi700052a.
11. **Mashhadi Z, Xu H, White RH.** 2009. An Fe^{2+}-dependent cyclic phosphodiesterase catalyzes the hydrolysis of 7,8-dihydro-D-neopterin 2′,3′-cyclic phosphate in methanopterin biosynthesis. Biochemistry **48:**9384–9392. http://dx.doi.org/10.1021/bi9010336.
12. **White RH.** 1990. Biosynthesis of methanopterin. Biochemistry **29:**5397–5404. http://dx.doi.org/10.1021/bi00474a027.
13. **White RH.** 1996. Biosynthesis of methanopterin. Biochemistry **35:**3447–3456. http://dx.doi.org/10.1021/bi952308m.
14. **Crécy-Lagard V, Phillips G, Grochowski LL, Yacoubi BE, Jenney F, Adams MW, Murzin AG, White RH.** 2012. Comparative genomics guided discovery of two missing archaeal enzyme families involved in the biosynthesis of the pterin moiety of tetrahydromethanopterin and tetrahydrofolate. ACS Chem. Biol. **7:**1807–1816. http://dx.doi.org/10.1021/cb300342u.
15. **Hennig M, D'Arcy A, Hampele IC, Page MG, Oefner C, Dale GE.** 1998. Crystal structure and reaction mechanism of 7,8-dihydroneopterin aldolase from *Staphylococcus aureus*. Nat. Struct. Biol. **5:**357–362. http://dx.doi.org/10.1038/nsb0598-357.
16. **Garcon A, Levy C, Derrick JP.** 2006. Crystal structure of the bifunctional dihydroneopterin aldolase/6-hydroxymethyl-7,8-dihydropterin pyrophosphokinase from *Streptococcus pneumoniae*. J. Mol. Biol. **360:**644–653. http://dx.doi.org/10.1016/j.jmb.2006.05.038.
17. **Goulding CW, Apostol MI, Sawaya MR, Phillips M, Parseghian A, Eisenberg D.** 2005. Regulation by oligomerization in a mycobacterial folate biosynthetic enzyme. J. Mol. Biol. **349:**61–72. http://dx.doi.org/10.1016/j.jmb.2005.03.023.
18. **Bauer S, Schott AK, Illarionova V, Bacher A, Huber R, Fischer M.** 2004. Biosynthesis of tetrahydrofolate in plants: crystal structure of 7,8-dihydroneopterin aldolase from *Arabidopsis thaliana* reveals a novel adolase class. J. Mol. Biol. **339:**967–979. http://dx.doi.org/10.1016/j.jmb.2004.04.034.
19. **Allen KN.** 1998. Reactions of enzyme-derived enamines, p 135–172. *In* Sinnott M (ed), Comprehensive biological catalysis. Academic Press, San Diego, CA.
20. **Gefflaut T, Blonski C, Perie J, Willson M.** 1995. Class I aldolases: substrate specificity, mechanism, inhibitors and structural aspects. Prog. Biophys. Mol. Biol. **63:**301–340. http://dx.doi.org/10.1016/0079-6107(95)00008-9.
21. **Fessner WD, Schneider A, Held H, Sinerius G, Walter C, Hixon M, Schloss JV.** 1996. The mechanism of class II, metal-dependent aldolases. Angew Chem. Int. Edit. **35:**2219–2221. http://dx.doi.org/10.1002/anie.199622191.
22. **Mathis JB, Brown GM.** 1970. The biosynthesis of folic acid. XI. Purification and properties of dihydroneopterin aldolase. J. Biol. Chem. **245:**3015–3025.
23. **Wang Y, Li Y, Yan H.** 2006. Mechanism of dihydroneopterin aldolase: functional roles of the conserved active site glutamate and lysine residues. Biochemistry **45:**15232–15239. http://dx.doi.org/10.1021/bi060949j.
24. **Wang Y, Li Y, Wu Y, Yan H.** 2007. Mechanism of dihydroneopterin aldolase. NMR, equilibrium and transient kinetic studies of the *Staphylococcus aureus* and *Escherichia coli* enzymes. FEBS J. **274:**2240–2252. http://dx.doi.org/10.1111/j.1742-4658.2007.05761.x.
25. **White RH, Xu H.** 2006. Methylglyoxal is an intermediate in the biosynthesis of 6-deoxy-5-ketofructose-1-phosphate: a precursor for aromatic amino acid biosynthesis in *Methanocaldococcus jannaschii*. Biochemistry **45:**12366–12379. http://dx.doi.org/10.1021/bi061018a.
26. **Bradford MM.** 1976. A rapid and sensitive method for the quantitation of microgram quantities of protein utilizing the principle of protein-dye

binding. Anal. Biochem. **72:**248–254. http://dx.doi.org/10.1016/0003-2697(76)90527-3.
27. **Czekster CM, Blanchard JS.** 2012. One substrate, five products: reactions catalyzed by the dihydroneopterin aldolase from *Mycobacterium tuberculosis*. J. Am. Chem. Soc. **134:**19758–19771. http://dx.doi.org/10.1021/ja308350f.
28. **Blaszczyk J, Li Y, Gan J, Yan H, Ji X.** 2007. Structural basis for the aldolase and epimerase activities of *Staphylococcus aureus* dihydroneopterin aldolase. J. Mol. Biol. **368:**161–169. http://dx.doi.org/10.1016/j.jmb.2007.02.009.
29. **Haussmann C, Rohdich F, Schmidt E, Bacher A, Richter G.** 1998. Biosynthesis of pteridines in *Escherichia coli*. Structural and mechanistic similarity of dihydroneopterin-triphosphate epimerase and dihydroneopterin aldolase. J. Biol. Chem. **273:**17418–17424.
30. **Wang Y, Scherperel G, Roberts KD, Jones AD, Reid GE, Yan H.** 2006. A point mutation converts dihydroneopterin aldolase to a cofactor-independent oxygenase. J. Am. Chem. Soc. **128:**13216–13223. http://dx.doi.org/10.1021/ja063455i.
31. **Jones WJ, Leigh JA, Mayer F, Woese CR, Wolfe RS.** 1983. *Methanococcus jannaschii* sp. nov., and extremely thermophilic methanogen from a submarine hydrothermal vent. Arch. Microbiol. **136:**254–261. http://dx.doi.org/10.1007/BF00425213.
32. **Wang YK, Morgan A, Stieglitz K, Stec B, Thompson B, Miller SJ, Roberts MF.** 2006. The temperature dependence of the inositol monophosphatase K_m correlates with accumulation of di-myo-inositol 1,1′-phosphate in *Archaeoglobus fulgidus*. Biochemistry **45:**3307–3314. http://dx.doi.org/10.1021/bi052467y.
33. **Kuliopulos A, Mildvan AS, Shortle D, Talalay P.** 1989. Kinetic and ultraviolet spectroscopic studies of active-site mutants of delta 5-3-ketosteroid isomerase. Biochemistry **28:**149–159. http://dx.doi.org/10.1021/bi00427a022.
34. **Brooks B, Benisek WF.** 1994. Mechanism of the reaction catalyzed by delta 5-3-ketosteroid isomerase of *Comamonas* (*Pseudomonas*) *testosteroni*: kinetic properties of a modified enzyme in which tyrosine 14 is replaced by 3-fluorotyrosine. Biochemistry **33:**2682–2687. http://dx.doi.org/10.1021/bi00175a042.
35. **Bohren KM, Grimshaw CE, Lai CJ, Harrison DH, Ringe D, Petsko GA, Gabbay KH.** 1994. Tyrosine-48 is the proton donor and histidine-110 directs substrate stereochemical selectivity in the reduction reaction of human aldose reductase: enzyme kinetics and crystal structure of the Y48H mutant enzyme. Biochemistry **33:**2021–2032. http://dx.doi.org/10.1021/bi00174a007.
36. **Choi KH, Lai V, Foster CE, Morris AJ, Tolan DR, Allen KN.** 2006. New superfamily members identified for Schiff-base enzymes based on verification of catalytically essential residues. Biochemistry **45:**8546–8555. http://dx.doi.org/10.1021/bi060239d.
37. **Elias M, Tawfik DS.** 2012. Divergence and convergence in enzyme evolution: parallel evolution of paraoxonases from quorum-quenching lactonases. J. Biol. Chem. **287:**11–20. http://dx.doi.org/10.1074/jbc.R111.257329.
38. **Kelley LA, Sternberg MJE.** 2009. Protein structure prediction on the Web: a case study using the Phyre server. Nat. Protoc. **4:**363–371. http://dx.doi.org/10.1038/nprot.2009.2.
39. **Pettersen EF, Goddard TD, Huang CC, Couch GS, Greenblatt DM, Meng EC, Ferrin TE.** 2004. UCSF Chimera—a visualization system for exploratory research and analysis. J. Comput. Chem. **25:**1605–1612. http://dx.doi.org/10.1002/jcc.20084.
40. **Trott O, Olson AJ.** 2010. AutoDock Vina: improving the speed and accuracy of docking with a new scoring function, efficient optimization, and multithreading. J. Comput. Chem. **31:**455–461. http://dx.doi.org/10.1002/jcc.21334.